Campbell J. Coghlan, Christopher J. Sumby and Christian J. Doonan

**Utilising hinged ligands in MOF synthesis: a covalent linking strategy for forming 3D MOFs**

CrystEngComm, 2014; 16(28):6364-6371



Published at: http://dx.doi.org/10.1039/c4ce00181h

Journal Name

RSCPublishing

ARTICLE

# Utilising Hinged Ligands in MOF Synthesis: A Covalent Linking Strategy for Forming 3D MOFs

Cite this: DOI: 10.1039/xoxxoooooox

Campbell J. Coghlan,[a] Christopher J. Sumby[a*] and Christian J. Doonan[a*]

Received ooth January 2012,
Accepted ooth January 2012

DOI: 10.1039/xoxxoooooox

www.rsc.org/

Here we show that connecting two equivalents of a bis-pyrazolymethane 'hinged' link via a carbon-carbon bond characteristically 'extends' the 2D layered metal-organic frameworks (MOFs) typically formed with such compounds into 3D MOF materials. 1,1,2,2-Tetrakis[4-(4-carboxyphenyl)-*1H*-pyrazol-1-yl]ethane (**L**) was prepared in three steps and upon reaction with late transition metals, namely copper(II), cadmium(II) and zinc(II), gave 3D MOFs $[Cu_2(\mathbf{L})(H_2O)_2]$ 1.4DMF and $[M_2\mathbf{L}]$·xDMF (M = Zn, x = 1; M = Cd, x = 1.75). The 3D MOFs display gating behaviour in their adsorption isotherms, consistent with 3rd generation flexible structures. Furthermore, the 3D MOFs showed appreciable affinity for $CO_2$ at 293 K however, due to the larger pore sizes molecular sieving of $CO_2/N_2$ was not observed. Reaction of **L** with cobalt(II) gave a 3D hydrogen-bonded network incorporating 1D coordination polymer chains that is topologically equivalent to the Zn and Cd MOFs. The strategy outlined here demonstrates a novel route for designing more chemically and thermally robust 3D MOFs from 2D layered materials.

## Introduction

Metal-organic frameworks (MOFs) are solid-state materials in which organic links of differing structure metrics and metal clusters are organized into extended networks with permanent porosity.[1-3] Structural flexibility in some MOFs - 3rd generation behaviour - provides additional properties arising from their dynamic structures that are not accessible to rigid materials.[3-7] The ability to systematically vary the structural design of these materials has led to applications for MOFs that extend to gas storage and separation,[8-10] drug delivery,[11] heterogeneous catalysis,[12] and microelectronics.[13]

Introducing structural flexibility into a MOF can be achieved by utilising non-rigid organic linkers,[14, 15] judicious choice of metal nodes[7, 16] or by the exploitation of non-covalent interactions in 2D layered and interpenetrated frameworks.[17-19] Recently, we introduced a strategy to reliably form flexible MOFs by designing a family of flexible organic links that possess a central chelating site.[20-22] Coordination of this central site modulates the flexibility of the organic link and gives rise to materials that routinely show 3rd generation behaviour. For example, a flexible silver(I) 3D material was formed using di-2-pyrazinylmethane (**dpzm**) as the organic building block; the material underwent solvent-induced expansion and contraction (breathing) upon exposure to different solvents.[20] Related ligands have also been studied by Du *et al.* as analogues of 4,4'-bipyridine.[23, 24] Extension of our work to an anionic link (Figure 1a, **bcppm**) gave a more chemically and thermally stable Cu(II) MOF, $[Cu(\mathbf{bcppm})(H_2O)]$ with outstanding $CO_2/N_2$ separation properties.[22] Of particular note was that this MOF underwent a structural transformation from a 2D flexible material to a 3D framework upon activation, with the 3D material having a rigid structure with pores capable of molecular sieving type separations.

2D layered MOFs (Figure 1c) often show phenomena such as layer-layer sliding and structure collapse on desolvation which has somewhat limited their use as porous materials.[3, 4, 25] To overcome such issues, a second organic building unit or 'pillaring link' is commonly used to construct 3D permanently porous materials[3, 4, 26] (Figure 1d). We speculated that close inspection of 2D layered structures could provide insight into how such pillars could, in selected cases, may be incorporated into the molecular architecture of the organic links. This approach can provide an efficient (one organic building unit) route to topologically related 3D materials. Motivated by the desirable properties of $[Cu(\mathbf{bcppm})(H_2O)]$,[22] here we demonstrate a strategy to covalently connect 2D MOFs by ligand design; i.e. synthetically installing a carbon-carbon connection between the 'hinges' of two equivalents of our flexible ligands[20-22] as a linking point between layers. This required us to design a new 'hinged' link (Figure 1b, **L**) that would facilitate covalent connection of 2D materials.

Here, we report a series of 3D MOFs constructed from the new 'hinged' link, 1,1,2,2-tetrakis[4-(4-carboxyphenyl)-*1H*-pyrazol-1-yl]ethane (**L**). Reactions of **L** with cadmium(II), copper(II) and zinc(II) gave materials topologically related to $[Cu(\mathbf{bcppm})(H_2O)]$ but where a 3D framework was formed by the linking of 2D layers through C-C covalent bonding. In addition, reaction of **L** with cobalt(II) resulted in the formation

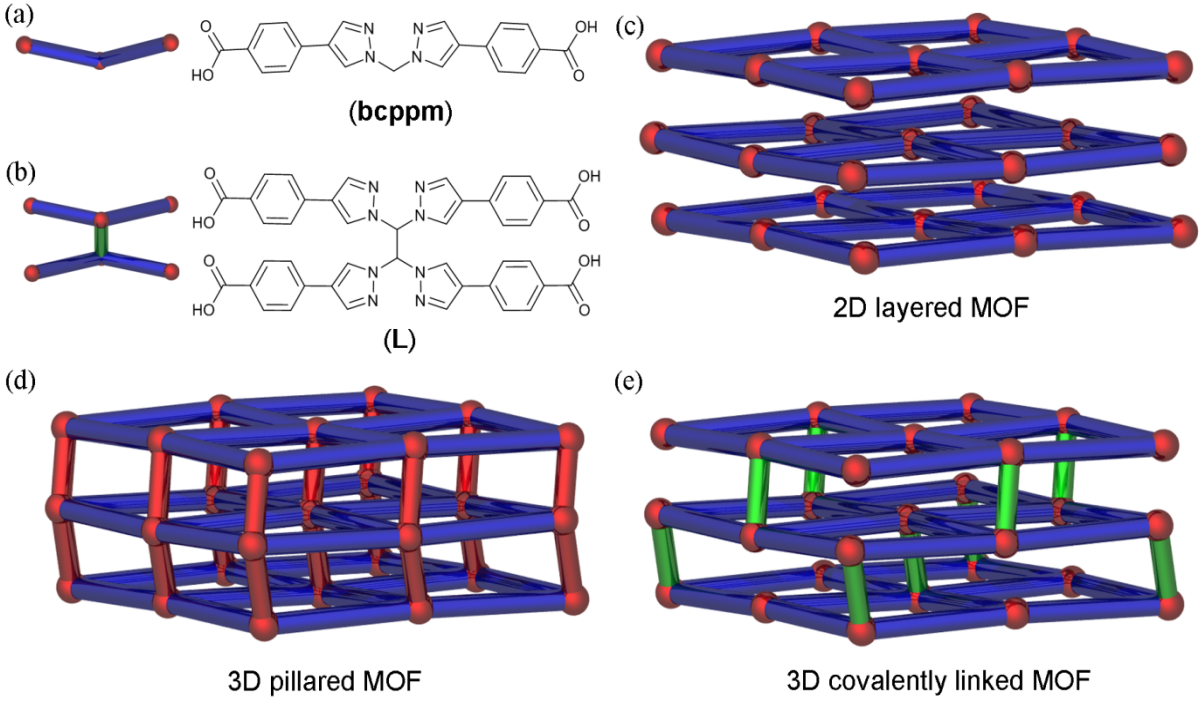


**Figure 1**. The structures of (a) **bcppm** and (b) **L** with schematic representations of the links showing the coordination modes present in MOFs containing these compounds (red spheres indicate coordinated metals and the green rod a carbon-carbon bond). Schematic representations of (c) 2D layered MOFs and two approaches used to form 3D MOFs, namely (d) pillaring ligands (red rods) and (e) covalent linking through carbon-carbon bonding (green rods).

of a topologically equivalent 3D hydrogen-bonded network. Herein, the structures, data on the chemical and thermal stability, and gas adsorption properties of all materials are reported.

## Experimental

### Materials and methods

All reagents, starting materials and solvents were purchased from Sigma-Aldrich or Boron Molecular and were used as received. 1,1,2,2-Tetrakis(4-iodo-*1H*-pyrazol-1-yl)ethane was prepared according to literature methods.[27] The Campbell microanalytical laboratory at the University of Otago, Dunedin performed all elemental analyses, Samples were activated before submission with adventitious water being observed in the analyses. NMR spectra were recorded on a Varian Gemini 600 spectrometer at 23°C using a 5 mm probe. Infrared (IR) spectra were recorded on a Perkin Elmer Fourier-Transform Infrared (FT-IR) spectrometer on a zinc-selenide crystal. Pore size calculations where done using Zeo++.[28] The analysis was conducted with the solvent removed and 2x2x2 super-cells of the crystal structures were used.

### Synthetic procedures

**1,1,2,2-Tetrakis[4-(4-carboxyphenyl)-*1H*-pyrazol-1-yl]ethane (L).** 1,1,2,2-Tetrakis(4-iodo-*1H*-pyrazol-1-yl)ethane (1.00 g, 1.25 mmol), 4-carboxyphenylboronic acid (1.25 g, 7.52 mmol) and aqueous $K_2CO_3$ (6.93 g in 40 mL of water) were combined in DMF (100 mL). After degassing with Ar for 30 mins, $Pd(PPh_3)_4$ (0.171 g, 0.15 mmol) was added, the mixture degassed for a further 30 mins and heated to 90°C for 24 hours. After cooling, the mixture was filtered, diluted with water (50 mL) and washed with dichloromethane (5 x 50 mL). Acidifying the aqueous layer with 20% $HNO_3$ (pH = 3) afforded a white solid which was isolated under reduced pressure, washed with ethanol and dried. Yield 763 mg (79%). M.p. 335-337°C. Found C 60.8, H 4.3, N 13.3, $C_{42}H_{36}N_8O_{11}$ (as trihydrate) requires: C 60.9, H 4.4, N 13.5%. $^1$H NMR (600 MHz/DMSO); δ 8.33 (s, 4H, PyrH), 8.07 (s, 4H, PyrH), 7.89 (d, 8H, ArH), 7.63 (d, 8H, ArH), 5.73 (s, 2H, CH). $^{13}$C NMR (600 MHz/DMSO): δ 166.9, 138.6, 135.7, 129.9, 127.0, 124.0, 121.8, 72.9. $\nu_{max}$ (neat, $cm^{-1}$): 2995 (-CH), 1686 (C=O), 1610 (C=N), 1566 (C=C).

**$[Cu_2(L)(H_2O)_2]\cdot 1.4DMF$.** In a screw cap vial, $Cu(NO_3)_2\cdot 2.5H_2O$ (6.5 mg, 0.022 mmol) and **L** (10.0 mg, 0.013 mmol) were combined and dissolved in DMF (1.5 mL) and water (1 mL). Acetic acid (2 drops) was added to the mixture and the mixture sonicated for 2 min. The mixture heated at 100°C for 2 days to give blue crystals of $[Cu_2(\mathbf{L})(H_2O)_2]$ 1.4DMF, which were washed three times with DMF. Yield 7.0 mg (60%, based on analysis for $[Cu_2(\mathbf{L})(H_2O)_2]\cdot 4H_2O$) Found C 50.2, H 3.7, N 11.4, $C_{42}H_{38}N_8O_{14}Cu_2$ requires: C 50.2, H 3.8, N 11.1%. $\nu_{max}$ (neat, $cm^{-1}$): 3094 (-CH), 1665 (C=O), 1595 (C=N), 1546 (C=C).

**$[Zn_2(L)]\cdot DMF$**. In a screw cap vial, $Zn(NO_3)_2\cdot 6H_2O$ (11.5 mg, 0.022 mmol) and **L** (10.0 mg, 0.013 mmol) were combined and dissolved in DMF (1.5 mL) and water (1 mL). Acetic acid (2

 

drops) was added to the mixture, the solution sonicated for 2 mins and heated at 100°C for 2 days. The resulting colourless crystals of [$Zn_2$(**L**)]·DMF were washed three times with DMF. Yield 9.0 mg (77% based on analysis for [$Zn_2$(**L**)]·4.5$H_2O$) Found C 47.1, H 3.4, N 10.6, $C_{42}H_{35}N_8O_{12.5}Zn_2$ requires: C 47.6, H 4.2, N 10.6%. $\nu_{max}$ (neat, $cm^{-1}$): 3087 (-CH), 1667 (C=O), 1597 (C=N), 1550 (C=C).

**[$Cd_2$(L)]·1.75DMF.** In a screw cap vial, $CdCl_2$.2.5$H_2O$ (4.73 mg, 0.022 mmol) and **L** (10 mg, 0.013 mmol) were combined and dissolved in DMF (1.5 mL) and water (1 mL). Acetic acid (2 drops) was added to the mixture and the mixture sonicated for 2 mins before being heated at 100°C for 2 days. The resulting colourless crystals were washed three times with DMF. Yield 9.0 mg (70% based on analysis for [$Cd_2$(**L**)]·5$H_2O$). Found C 46.4, H 3.0, N 10.7, $C_{42}H_{36}N_8O_{13}Cd_2$ requires: C 46.5, H 3.3, N 10.3%. $\nu_{max}$ (neat, $cm^{-1}$): 3083 (-CH), 1670 (C=O), 1612 (C=N), 1579 (C=C).

**[$Co_2$(L)($H_2O$)$_6$]·DMF.** In a screw cap vial, $Co(NO_3)_2$.6$H_2O$ (3.75 mg, 0.022 mmol) and **L** (10.0 mg, 0.013 mmol) were combined and dissolved in DMF (1.5 mL) and water (1 mL). Acetic acid (2 drops) was added to the mixture and the mixture sonicated for 2 mins before being heated at 85°C for 2 days. The resulting pink crystals were washed three times with DMF. Yield 8.0 mg (69% based on analysis for [$Co_2$L($H_2O$)$_6$].5$H_2O$). Found C 46.8, H 4.0, N 9.7, $C_{42}H_{48}N_8O_{19}Co_2$ requires: C 46.4, H 4.4, N 10.3%. $\nu_{max}$ (neat, $cm^{-1}$): 3095 (br, OH), 1630 (C=O), 1579 (C=N), 1527 (C=C).

### X-Ray Crystallography

Single crystals were mounted in paratone-N oil on a plastic loop. X-ray diffraction data were collected at low temperature with MoKα radiation (λ = 0.7107 Å) using an Oxford Diffraction X-calibur single-crystal X-ray diffractometer ([$Cu_2$(**L**)($H_2O$)$_2$]·1.4DMF, [$Cd_2$(**L**)]·1.75DMF and [$Co_2$(**L**)($H_2O$)$_6$]·DMF) or on the MX1 beamline of the Australian Synchrotron (λ = 0.7107 Å, [$Zn_2$(**L**)]·DMF). Data sets were corrected for absorption using multi-scan methods, and structures were solved by direct methods using SHELXS-97[29] and refined by full-matrix least-squares on $F^2$ by SHELXL-97,[30] interfaced through the program X-Seed.[31] In general, all non-hydrogen atoms were refined anisotropically and hydrogen atoms were included as invariants at geometrically estimated positions, unless specified otherwise in additional details below. Figures were produced using the program POV-Ray.[32] Crystallographic parameters for the structures are given in Table 1. CCDC 980812-980815 contain the supplementary crystallographic data for these structures. These data can be obtained free of charge from The Cambridge Crystallographic Data Centre via www.ccdc.cam.ac.uk/data_request/cif.

**Additional refinement details for [$Cu_2$(L)($H_2O$)$_2$]·1.4DMF.** The hydrogen atoms on the coordinated water molecule could not be located in the difference map and were not included in the model. The structure contained large solvent accessible voids and the SQUEEZE[33] routine of Platon[34] was applied to the data. Electron density corresponding to approximately 1.4 DMF per asymmetric unit was removed (462 electrons per unit cell) and this was included in the formula for the crystal structure.

**Additional refinement details for [$Zn_2$(L)]·DMF, [$Cd_2$(L)]·1.75DMF and [$Co_2$(L)($H_2O$)$_6$]·DMF.** These structures contained large solvent accessible voids and the SQUEEZE[33] routine of Platon[34] was applied to the data. Electron density corresponding to approximately 1, 1.75, and 1 DMF molecule per asymmetric unit was removed (268, 552, and 264 electrons per unit cell), respectively. These solvates were included in the formulae for the crystal structures.

### Powder X-ray Diffraction

Powder X-ray diffraction data was collected on a Bruker D8 Advance diffractometer using Cu-Kα radiation. Samples were prepared in 0.5 mm quartz glass capillaries.

**Table 1.** Selected crystallographic parameters for [$Cu_2$(**L**)($H_2O$)$_2$]·1.4DMF, [$Zn_2$(**L**)]·DMF, [$Cd_2$(**L**)]·1.75DMF and [$Co_2$(**L**)($H_2O$)$_6$]·DMF.

| Compound | [$Cu_2$(**L**)($H_2O$)$_2$] 1.4DMF | [$Zn_2$(**L**)]·DMF | [$Cd_2$(**L**)]·1.75DMF | [$Co_2$(**L**)($H_2O$)$_6$]·DMF |
|---|---|---|---|---|
| Formula | $C_{14.7}H_{17.3}Cu_{0.5}N_{3.4}O_{3.9}$ | $C_{24}H_{20}N_5O_5Zn$ | $C_{26.25}H_{25.25}CdN_{5.75}O_{5.75}$ | $C_{13.5}H_{16.5}Co_{0.5}N_3O_{4.5}$ |
| Crystal system | Orthorhombic | Monoclinic | Monoclinic | Orthorhombic |
| Space group | *Pnnm* | *C2/c* | *C2/c* | *Pnnm* |
| *a*/Å | 11.9272(15) | 23.269(5) | 23.324(3) | 10.0477(3) |
| *b*/Å | 13.954(3) | 10.602(2) | 10.2514(6) | 15.2023(10) |
| *c*/Å | 20.185(2) | 24.340(5) | 25.426(2) | 22.6589(7) |
| *β*/° | | 111.28(3) | 116.190(15) | |
| *V*/Å$^3$ | 3359.4(9) | 5595.1(19) | 5455.3(9) | 3461.1(3) |
| *ρ*/g cm$^{-3}$ | 1.328 | 1.244 | 1.524 | 1.237 |
| *Z* | 8 | 8 | 8 | 8 |
| *T*/K | 150 | 100 | 110 | 109 |
| *μ*/mm$^{-1}$ | 0.706 | 0.916 | 0.850 | 0.549 |
| Reflections collected | 14847 | 38075 | 23055 | 13993 |
| Unique reflections ($R_{int}$) | 4172 (0.1017) | 5463 (0.0331) | 5356 (0.0866) | 3132 (0.0547) |
| Reflections $I>2\sigma(I)$ | 1670 | 4853 | 3843 | 2418 |
| Data/Restraints/ Parameters | 4172 / 0 / 145 | 5463 / 0 / 271 | 3843 / 0 / 271 | 3132 / 4 / 166 |
| Goodness of fit (S) | 0.994 | 1.088 | 1.035 | 1.090 |
| *R*1/*wR*2 [$I>2\sigma(I)$] | 0.1268 / 0.3509 | 0.0706 / 0.1961 | 0.0619 / 0.1366 | 0.0574 / 0.1698 |
| *R*1/*wR*2 (all data) | 0.2069 / 0.3828 | 0.0767 / 0.2007 | 0.0933 / 0.1476 | 0.0755 / 0.1791 |

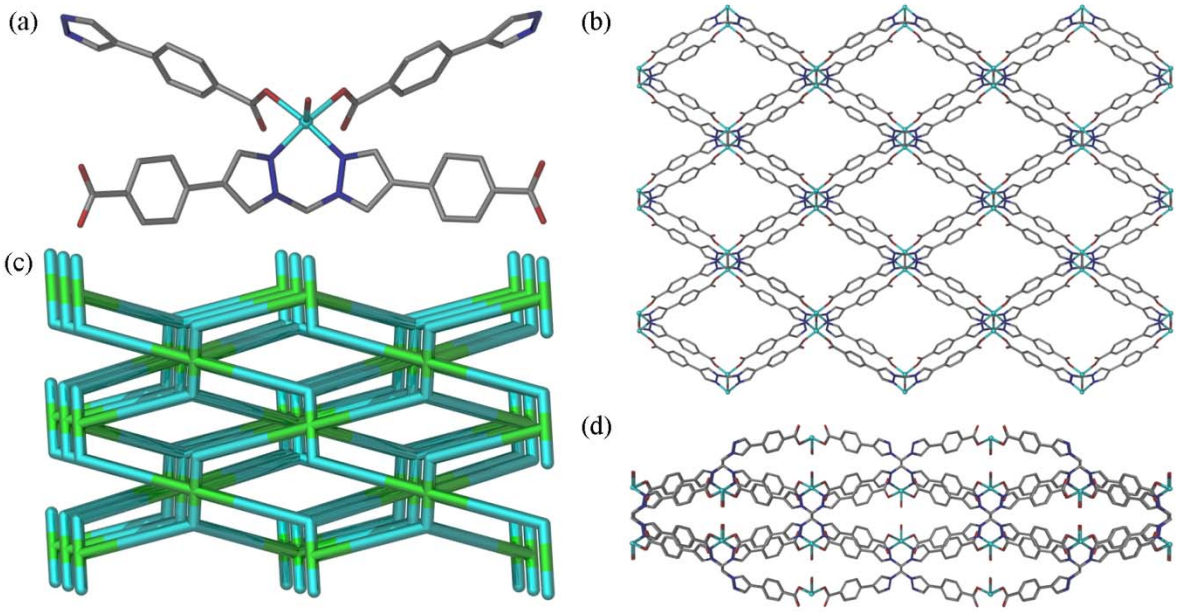


**Figure 2**. (a) The coordination environment around the Cu centre in $[Cu_2(\mathbf{L})(H_2O)_2]$ 1.4DMF. Views of $[Cu_2(\mathbf{L})(H_2O)_2]$ 1.4DMF (b) along the *a*-axis, (c) an equivalently orientated topological representation along the *a*-axis (Cu centres as 3-connecting centres, shown in blue, and the ligands as 6 connecting centres, shown in green) and (d) a structural representation shown looking along the *b*-axis. Hydrogen atoms omitted for clarity.

## Results and discussion

### Ligand and MOF Synthesis

The organic linker 1,1,2,2-tetrakis[4-(4-carboxyphenyl)-*1H*-pyrazol-1-yl]ethane (**L**) was readily synthesised from 1,1,2,2-tetrakis(4-iodo-*1H*-pyrazol-1-yl)ethane[27] and 4-carboxyphenylboronic acid (Chart 1) via a Suzuki coupling in 79% yield. Compound **L** maintains the design features present in **bcppm**,[22] namely flexibility derived from the methylene hinge, anionic O-donors and a bidentate chelating site. In contrast, **L** contains a C-C bond between the two dipyrazole moieties (see ESI, Chart S1, for an illustration of the coordination modes encountered in this work). Using the 2D layered structure of [Cu(**bcppm**)($H_2O$)] as a blueprint, we posited that this substitution of the solvent 'pillar' with a C-C bond would afford a topologically related robust 3D network.

Solvothermal reactions of **L** with $Cu(NO_3)_2{\cdot}2.5H_2O$, $Zn(NO_3)_2{\cdot}6H_2O$, $Co(NO_3)_2{\cdot}6H_2O$ and $CdCl_2{\cdot}2.5H_2O$ in mixtures of DMF/$H_2O$ and AcOH (or $HNO_3$) to improve crystal growth gave X-ray quality crystals of $[Cu_2(\mathbf{L})(H_2O)_2]$ 1.4DMF, $[Zn_2(\mathbf{L})]{\cdot}$DMF, $[Co_2(\mathbf{L})(H_2O)_6]{\cdot}$DMF and $[Cd_2(\mathbf{L})]{\cdot}$1.75DMF after 24 hours (Table 1).[7] IR spectroscopy revealed that the band for the C=O stretch of the ligand was shifted from 1686 $cm^{-1}$ for the free ligand to shorter wavenumbers (1665 – 1670 $cm^{-1}$) in the MOFs and 1630 $cm^{-1}$ in the hydrogen-bonded network $[Co_2(\mathbf{L})(H_2O)_6]$ providing an excellent handle on the nature of bonding in the four materials.

### Crystal Structures

As anticipated, incorporating a C-C bond to link together two bis-pyrazolymethane 'hinged' moieties led to the formation of a 3D MOF material, $[Cu_2(\mathbf{L})(H_2O)_2]$ 1.4DMF. Like [Cu(**bcppm**)($H_2O$)],[22] $[Cu_2(\mathbf{L})(H_2O)_2]$ 1.4DMF has a square pyramidal Cu(II) centre which is coordinated by a dipyrazole chelating unit from a molecule of **L** (Cu-N bond length of 1.987(6) Å), two symmetry-related monodentate carboxylate oxygen donors from two further molecules of **L** (Cu-O bond length of 1.970(5) Å) and a single water ligand with a bond length of 2.312(12) Å (Figure 2a). Without the C-C connection from the ligand the material has a 2D 4-connected structure (akin to [Cu(**bcppm**)($H_2O$)] when one treats each [Cu(**bcppm**)] moiety as a 4-conecting centre). However, the presence of a C-C bond in **L** has several important structural ramifications, including the obvious extension of the material to a 3D structure (Figure 2b and 2c) as proposed (Figure 1e). Unlike the previously reported material (Figure 1c), the carbonyl oxygen atoms are not hydrogen bonded to the water molecule on an adjacent metal atom; instead they form weaker C-H···O bonds with the CH of the ethane link in **L**.

$[Cu_2(\mathbf{L})(H_2O)_2]$ 1.4DMF possesses diamond-shaped channels aligned coincident with the *a*-axis of the unit cell (Figure 2b). These measure ~13.9 by 20.2 Å between Cu centres, with a calculated maximum pore size in the order of 7.9 Å at their narrowest point using Zeo++.[28] This is larger than the similarly shaped channels in [Cu(**bcppm**)($H_2O$)]. The 'layer' separations are dictated by the C-C bonds of **L** resulting in a Cu-Cu separation of either ~6.0 or 6.6 Å (the former between Cu centres where the water ligands of both Cu centres are hydrogen bonded and the latter between Cu centres bridged by a molecule of **L**, Figure 2d). These moieties alternate at the apices of each diamond-shaped channel in the *a*-axis direction. In a more formal topological treatment, viewing the Cu centres as 3-connecting nodes and the ligand as a 6-connecting node (it

 

coordinates two Cu centres with the dipyrazole donors and four Cu centres with monodentate carboxylate donors) gives a binodal 3,6-connected net with a commonly encountered rutile-type topology. However, the MOF is perhaps better considered as a partially linked 2D layered material.[35]

The Zn analogue forms a closely related 3D MOF, with the major distinction between the $[Cu_2(\mathbf{L})(H_2O)_2]$ 1.4DMF and $[Zn_2(\mathbf{L})]$·DMF structures being the replacement of the apical water ligand by a carboxylate oxygen from an adjacent layer. This zinc(II) dimer secondary building unit (SBU), which provides another layer-layer connection, dramatically distorts the 2D 'layers' and provides a closer metal-metal distance (~3.8 Å) for the bridged zinc(II) centres (vs. 6.0 Å in $[Cu_2(\mathbf{L})(H_2O)_2]$ 1.4DMF). The zinc(II) centre adopts a distorted square pyramidal geometry and is coordinated by a dipyrazole unit from a molecule of **L**, a monodentate carboxylate and two bridging carboxylate oxygen donors (Figure 3a). To provide this bridging motif one of the carboxylate ligands is twisted away from the type of C-H···O hydrogen bonding interaction present in $[Cu_2(\mathbf{L})(H_2O)_2]$ 1.4DMF. In terms of the pore structure, a very similar packing to that present in $[Cu_2(\mathbf{L})(H_2O)_2]$ 1.4DMF gives rise to diamond-shaped channels directed along the *b*-axis with a pore diameter of ~6.6 Å (Zn-Zn separations of 13.5 and 18.9 Å, Figure 3c; side view Figure 3d). Topologically however the presence of an additional layer-to-layer contact in the form of the zinc SBU means that, along with the C-C bond of **L**, the MOF contains two topologically equivalent 6-connecting nodes and hence a binodal 6-connected net (Figures 3e). This additional layer-layer connection provides a 3D MOF with a structure more akin to the pillared 3D MOFs (Figure 1d) rather than the simple, covalently linked structure (Figure 1e).

$[Cd_2(\mathbf{L})]$·1.75DMF is also a 3D MOF and is isomorphous but not strictly isostructural with $[Zn_2(\mathbf{L})]$·DMF. In a similar manner to $[Zn_2(\mathbf{L})]$·DMF, the cadmium(II) centres form a dimer which are bridged by two $\mu_2$-carboxylate oxygen atoms from the carboxylic acid moieties of **L**. However, the cadmium(II) centres are 7-coordinate and are coordinated by two pyrazole nitrogen atoms, two chelating carboxylic acids and a monodentate carboxylate (that chelates a second Cd centre, Figure 3b). A very similar packing to that present in $[Cu_2(\mathbf{L})(H_2O)_2]$ 1.4DMF and $[Zn_2(\mathbf{L})]$·DMF gives rise to diamond-shaped channels directed along the *b*-axis with a pore diameter of ~6.4 Å (Cd-Cd separations of 13.7 and 19.4 Å about the channel). $[Zn_2(\mathbf{L})]$·DMF and $[Cd_2(\mathbf{L})]$·1.75DMF are topologically identical (Figure 3e).

$[Co_2(\mathbf{L})(H_2O)_6]$·DMF has a very similar overall 3D structure in terms of topology to both the zinc(II) and cadmium(II) materials but, due to additional coordination of the Co(II) centres by water ligands, only possesses a 1D coordination polymer structure that is hydrogen-bonded to form a commensurate 3D network. The cobalt centre (Figure 4a) is coordinated by a dipyrazole unit from a molecule of **L** (Co-N 2.126(3) Å) and four water ligands; two in axial position (Co-O 2.063(4) and 2.077(4) Å) and two $\mu_2$-aquo ligands that bridge to a second Co centre (Co-O 2.125(2) Å). The dimeric Co(II) moiety is coordinated by two different molecules of **L** which give rise to a 1D coordination polymer that extends along the *a*-axis of the unit cell (Figure 4b). Each of the carboxylates that radiate out from these 1D chains form two strong hydrogen

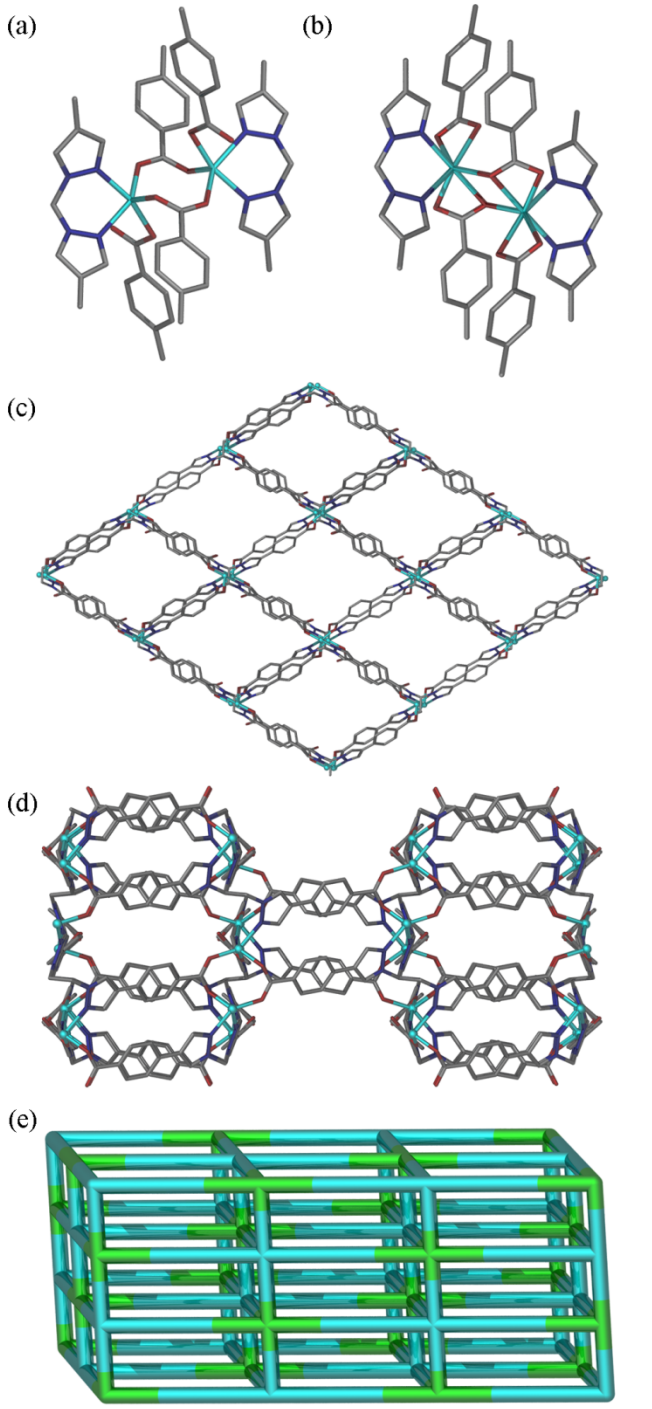


**Figure 3**. The coordination environments around (a) the Zn(II) dimers and (b) the Cd(II) dimers in the 3D MOFs (hydrogen atoms omitted). The structure of $[Zn_2(\mathbf{L})]$·DMF looking (c) down the *b*-axis and (d) down the *c*-axis. (e) The underlying binodal 6-connecting network topology in $[Zn_2(\mathbf{L})]$·DMF and $[Cd_2(\mathbf{L})]$·1.75DMF with nodes comprising the 6-connecting the M(II) dimer unit and **L** shown in aqua and bright green, respectively.

bonds (O-H···O; D = 2.50, 2.64 Å, d = 1.63, 1.78 Å, angle = 156.2, 164.5°) with the water ligands of an adjacent 1D coordination polymer to form a 3D hydrogen bonded network. The hydrogen bonded network of $[Co_2(\mathbf{L})(H_2O)_6]\cdot DMF$ possesses diamond-shaped channels, much like the Cu, Zn and Cd MOFs, aligned coincident with the *a*-axis of the unit cell (Figure 4c). Due to the hydrogen bonding these are larger than the equivalent channels in the 3D MOFs and measure ~15.2 by 22.7 Å between Co centres and the largest maximum pore diameter for this series of materials of 8.5 Å.

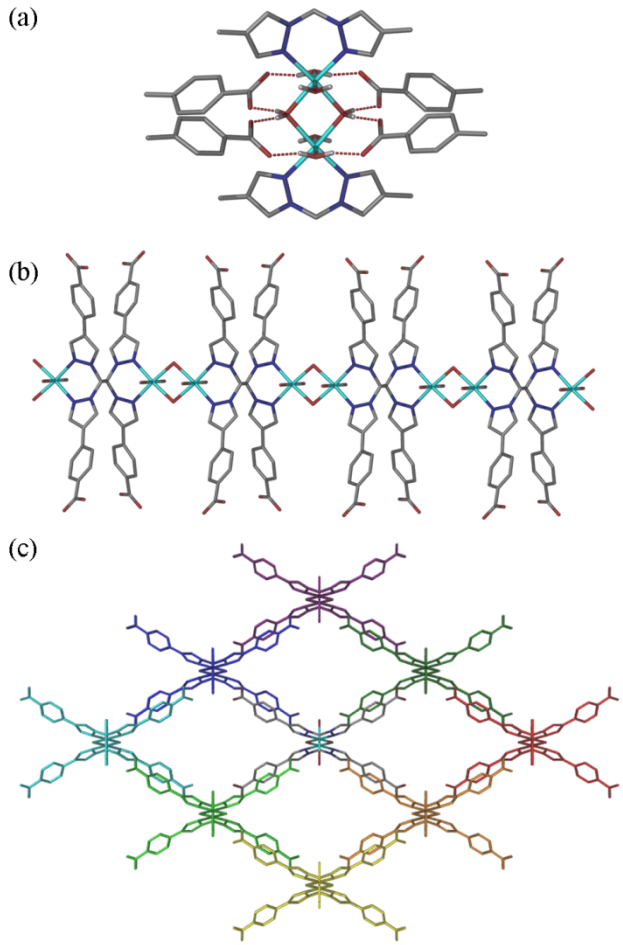


**Figure 4**. (a) The coordination and hydrogen bonding environment of the Co centres in $[Co_2(\mathbf{L})(H_2O)_6]\cdot DMF$ (hydrogen atoms not on the water ligands omitted for clarity. A view of the (b) 1D coordination polymers and (c) the 3D hydrogen bonded network in $[Co_2(\mathbf{L})(H_2O)_6]\cdot DMF$ (hydrogen atoms omitted for clarity). Individual 1D coordination polymers are shown in different colours with the central example in a CPK colour scheme.

Despite possessing quite different 3D connectivity (hydrogen bonding vs. covalent bonds), all of the structures showed good thermal stability of over 400°C (275°C for $[Cu_2(\mathbf{L})(H_2O)_2]$ 1.4DMF) as shown by their respective thermogravimetric analysis traces (see ESI, Figure SI 1). PXRD (see ESI, Figures SI 2-5) indicated that the four materials remained crystalline following activation although, as is known for 3rd generation materials, the materials underwent structural changes that occur upon guest removal, likely to be a trellis-like expansion/contraction process akin to that seen in related materials.[22] This observation is supported by pore size distributions and gating in the 77 K $N_2$ and 195 K $CO_2$ adsorption isotherms discussed below. Given that the carbon-carbon connection from the ligand in these 3D MOF materials was expected to yield more chemically robust frameworks, we sought to investigate their stability towards moisture. Previously activated samples of the Zn(II) MOF were stirred in $H_2O$ at room temperature, 50°C and 85°C for 24 hours. PXRD of the samples reactivated from MeOH showed minimal loss of crystallinity (Figure 5).

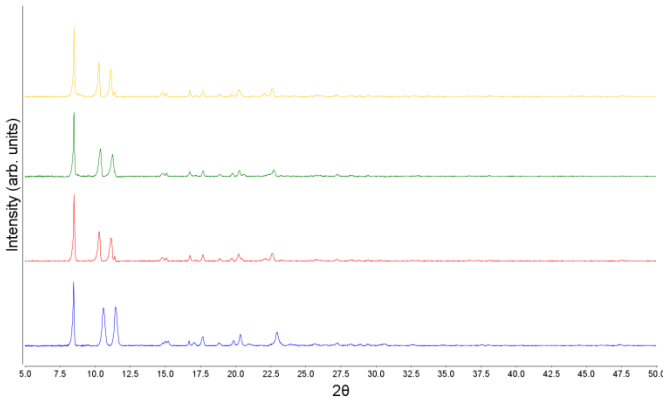


**Figure 5**. PXRD patterns for $[Zn_2(\mathbf{L})]$. Original, activated sample (blue trace). Samples reactivated from MeOH after being in water for 24 hrs at room temperature (red), 50°C (green) and 85°C (yellow).

### Gas Absorption and Structural Flexibility

All four activated materials ($[Cu_2(\mathbf{L})(H_2O)_2]$, $[Zn_2(\mathbf{L})]$, $[Co_2(\mathbf{L})(H_2O)_6]$ and $[Cd_2(\mathbf{L})]$) were shown to be porous to both $N_2$ and $CO_2$ at several temperatures. From the 77 K $N_2$ isotherms BET surface areas and pore size distributions were calculated (Table 2). Despite having similar structures, subtle differences in the layer-layer separations and chemistry around the metal centres may account for the differences observed. $[Cu_2(\mathbf{L})(H_2O)_2]$, $[Zn_2(\mathbf{L})]$ and $[Cd_2(\mathbf{L})]$ all have one larger pore size which is consistent with the diamond-shaped pores present in their structures. $[Co_2(\mathbf{L})(H_2O)_6]$ lacks the larger pore size observed for the three 3D MOFs which presumably arises from more pronounced contraction (flattening) of the diamond-shaped windows due to greater flexibility within the hydrogen-bonded 3D structure.

**Table 2**. BET surface areas and pore sizes for $[Cu_2(\mathbf{L})(H_2O)_2]$, $[Zn_2(\mathbf{L})]$, $[Cd_2(\mathbf{L})]$, $[Co_2(\mathbf{L})(H_2O)_6]$ and $[Cu(\mathbf{bcppm})(H_2O)]$.

| | BET surface area ($m^2/g$) | Experimental pore sizes (Å)[a] |
|---|---|---|
| $[Cu_2(\mathbf{L})(H_2O)_2]$ | 844.5 | 10.9 |
| $[Zn_2(\mathbf{L})]$ | 1075.4 | 10.9 |
| $[Cd_2(\mathbf{L})]$ | 571.7 | 10.9 |
| $[Co_2(\mathbf{L})(H_2O)_6]$ | 734.6 | 5.9, 6.8 |
| $[Cu(\mathbf{bcppm})(H_2O)]$[22] | 155 | 3.6 |

[a] See ESI, Figure SI 8.

Figure 6 shows that gating behaviour is present in the 195 K $CO_2$ isotherms for the three MOFs, [$Cu_2$(**L**)($H_2O$)$_2$], [$Zn_2$(**L**)] and [$Cd_2$(**L**)]. This reveals that the materials retain structural flexibility upon activation and do not form a rigid structure as observed for [Cu(**bcppm**)($H_2O$)] upon heating,[22] i.e. the materials retain 3rd generation behavior.[3-5] Based on previous studies,[20-22] it is likely that the gating originates from a trellis-like structural change, i.e. expansion in one axis across the diamond-shaped pores and contraction across the other. In contrast, the cobalt(II) material remains in a 'locked' form and does not display the features of gating in its 77 K $N_2$ isotherm.

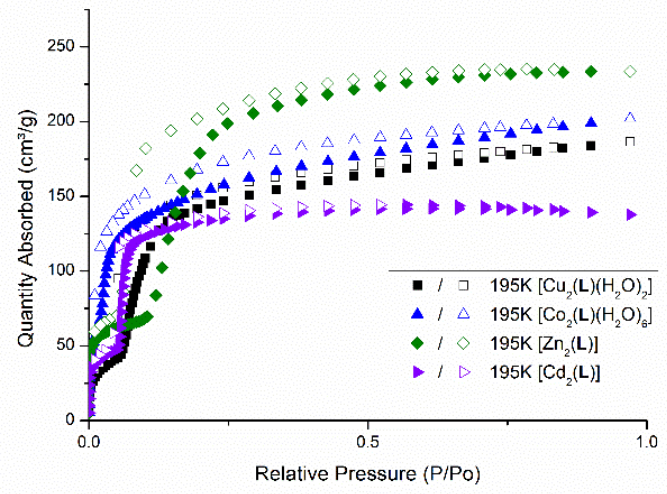


**Figure 6**. 195 K $CO_2$ isotherms for [$Cu_2$(**L**)($H_2O$)$_2$], [$Zn_2$(**L**)], [$Cd_2$(**L**)] and [$Co_2$(**L**)($H_2O$)$_6$].

Previously we showed exceptional $CO_2/N_2$ separation for a closely related MOF material, [Cu(**bcppm**)($H_2O$)]. This material had diamond-shaped channels with pore dimensions of *ca.* 3.6 Å in the activated form that remain locked upon gas adsorption.[22] To put this result into context, we investigated the $CO_2$ and $N_2$ adsorption of the four materials reported here at room temperature (see ESI Figure SI 6). The three 3D MOFs showed appreciable $CO_2$ uptake at low pressure with [$Zn_2$(**L**)] showing the highest uptake amongst the MOF materials (57.5 $cm^3/g$). [$Co_2$(**L**)($H_2O$)$_6$] displayed little affinity for $CO_2$, but had the highest overall uptake of $CO_2$ (57.5 $cm^3/g$). The considerably larger pore dimensions (Table 2) of the materials reported here compared with [Cu(**bcppm**)($H_2O$)] results in a greater absorption capacity but a lower selectivity for $CO_2$ over $N_2$ due to the unrestricted pore dimensions of these materials.[22, 36, 37] However, due to the considerably larger experimental surface areas and pore sizes, all materials absorb considerably more $CO_2$ than [Cu(**bcppm**)($H_2O$)].

## Conclusions

Herein, we have reported four new materials which extends our previous work utilising 'hinged' organic building blocks to synthesise flexible MOFs. A new organic building block, 1,1,2,2-tetrakis[4-(4-carboxyphenyl)-*1H*-pyrazol-1-yl]ethane, was synthesised in high yield with the intention of covalently linking the types of 2-D layers present in the predecessor MOF, [Cu(**bcppm**)($H_2O$)], while still maintaining a degree of structural flexibility. All the four materials showed high thermal stability and the three MOFs retained structural flexibility upon activation validating our aim of covalently linking layers to achieve more robust 3D MOFs.

Reaction of **L** with cobalt(II) gave [$Co_2$(**L**)($H_2O$)$_6$]·DMF, a 1-D polymer linked together into a 3-D network through hydrogen bonding. This particular material did not show any gating behaviour in its adsorption isotherms or any particular affinity for $CO_2$ at 293 K despite possessing the highest overall uptake. Copper(II), zinc(II) and cadmium(II) salts all formed flexible 3D MOFs, [$Cu_2$(**L**)($H_2O$)$_2$] 1.4DMF, [$Zn_2$(**L**)]·DMF and [$Cd_2$(**L**)]·1.75DMF, which displayed gating in their 77 K $N_2$ and 195 K $CO_2$ isotherms consistent with 3rd generation structures. Furthermore, all 3D MOFs displayed a larger pore dimension consistent with the diamond-shaped channels which are a characteristic of this family of materials. At 293 K these MOFs showed good low pressure affinity for $CO_2$ and a reasonable overall uptake.

## Acknowledgements

CJD and CJS gratefully acknowledge the Science and Industry Endowment Fund for financial support and the Australian Research Council for funding Future Fellowships (FT100100400 and FT0991910). Aspects of this research were undertaken on the MX1 beamline at the Australian Synchrotron, Victoria, Australia. Dr Witold Bloch and Mr Jack Evans are thanked for helpful discussions regarding the manuscript.

## Notes and references

[a] *Centre for Advanced Nanomaterials, School of Chemistry & Physics, The University of Adelaide, Adelaide, Australia. CJD: Tel: +61 8 8313 5770; Fax: +61 8 8313 4358; E-mail: christian.doonan@adelaide.edu.au, CJS: Tel: +61 8 8313 7406. Fax. +61 8 8313 4358. E-mail: christopher.sumby@adelaide.edu.au*

Electronic Supplementary Information (ESI) available: Thermogravimetric analysis results, PXRD data, and gas adsorption isotherms for [$Cu_2$(**L**)($H_2O$)$_2$], [$Zn_2$(**L**)], [$Cd_2$(**L**)] and [$Co_2$(**L**)($H_2O$)$_6$]. See DOI: 10.1039/b000000x/

1. T. R. Cook, Y.-R. Zheng and P. J. Stang, *Chem. Rev.*, 2013, **113**, 734-777.
2. G. Ferey, *Chem. Soc. Rev.*, 2008, **37**, 191-214.
3. S. Kitagawa, R. Kitaura and S.-i. Noro, *Angew. Chem. Int. Ed.*, 2004, **43**, 2334-2375.
4. S. Kitagawa and K. Uemura, *Chem. Soc. Rev.*, 2005, **34**, 109-119.
5. S. Horike, S. Shimomura and S. Kitagawa, *Nat. Chem.*, 2009, **1**, 695-704.
6. C. Serre and G. Feney, *Chem. Soc. Rev.*, 2009, **38**, 1380-1399.
7. C. Serre, F. Millange, M. Thouvenot, N. M., G. Marsolier, D. Louer and G. Feney, *J. Am. Chem. Soc.*, 2002, **124**, 13519-13526.

8. D. Britt, D. Tranchemontagne and O. M. Yaghi, *Proc. Natl. Acad. Sci.*, 2008, **105**, 11623-11627.
9. K. Sumida, D. L. Rogow, J. A. Mason, T. M. McDonald, E. D. Bloch, Z. R. Herm, T.-H. Bae and J. R. Long, *Chem. Rev.*, 2012, **112**, 724-781.
10. J. Liu, P. K. Thallapally, B. P. McGrail, D. R. Brown and J. Liu, *Chem. Soc. Rev.*, 2012, **41**, 2308-2322.
11. P. Horcajada, T. Chalati, C. Serre, B. Gillet, C. Sebrie, T. Baati, J. F. Eubank, D. Heurtaux, P. Clayette, C. Kreuz, J.-S. Chang, Y. K. Hwang, V. Marsaud, P.-N. Bories, L. Cynober, S. Gil, G. Ferey, P. Couvreur and R. Gref, *Nat. Mater.*, 2010, **9**, 172-178.
12. I. H. Hwang, J. M. Bae, W.-S. Kim, Y. D. Jo, C. Kim, Y. Kim, S.-J. Kim and S. Huh, *Dalton Trans.*, 2012, **41**, 12759-12765.
13. K. Zagorodniy, G. Seifert and H. Hermann, *Appl. Phys. Lett.*, 2010, **97**, 251905/251901-251905/251902.
14. H.-S. Choi and M. P. Suh, *Angew. Chem. Int. Ed.*, 2009, **48**, 6865-6869.
15. M. P. Suh and T. K. Kim, *Chem. Commun.*, 2011, **47**, 4258-4260.
16. C. Serre, C. Mellot-Draznieks, S. Surble, N. Audebrand, Y. Filinchuk and G. Feney, *Science*, 2007, **315**, 1828-1831.
17. H. J. Park and M. P. Suh, *Chem. Commun.*, 2010, **48**, 610-612.
18. K. Uemura, S. Kitagawa, K. Fukui and K. Saito, *J. Am. Chem. Soc.*, 2004, **126**, 3817-3828.
19. T. K. Maji, R. Matsuda and S. Kitagawa, *Nat. Mater.*, 2007, **6**, 142-148.
20. W. M. Bloch and C. J. Sumby, *Chem. Commun.*, 2012, **48**, 2534-2536.
21. W. M. Bloch, C. J. Doonan and C. J. Sumby, *CrystEngComm*, 2013, **15**, 9663-9671.
22. W. M. Bloch, R. Babarao, M. R. Hill, C. J. Doonan and C. J. Sumby, *J. Am. Chem. Soc.*, 2013, **135**, 10441-10448.
23. M. Du, X.-G. Wang, Z.-H. Zhang, L.-F. Tang and X.-J. Zhao, *CrystEngComm*, 2006, **8**, 788-793
24. M. Du, Z.-H. Zhang, X.-G. Wang, L.-F. Tang and X.-J. Zhao, *CrystEngComm*, 2008, **10**, 1855-1865
25. K. Biradha, Y. Hongo and M. Fujita, *Angew. Chem. Int. Ed.*, 2002, **41**, 3395-3398.
26. G. K. Kole and J. J. Vittal, *Chem. Soc. Rev.*, 2013, **42**, 1755-1775.
27. E. A. Nudnova, A. S. Potapov, A. I. Khlebnikov and V. D. Ogorodnikov, *Russ. J. Org. Chem.*, 2007, **43**, 1698-1702.
28. T. F. Willems, C. H. Rycroft, M. Kazi, J. C. Meza and M. Haranczyk, *Micropor. Mesopor. Mat.*, 2012, **149**, 134-141.
29. G. M. Sheldrick, *Acta Crystallogr., Section. A*, 1990, **46**, 467-473.
30. G. M. Sheldrick, SHELXL-97, University of Göttingen, Göttingen, Germany, 1997.
31. L. J. Barbour, *J. Supramol. Chem.*, 2003, **1**, 189-191.
32. PoVRay 3.6, Persistence of Vision Pty. Ltd., Williamstown, Victoria, Australia, 2004.
33. A. L. Spek, *Acta Crystallogr., Section A*, 1990, **46**, C34.
34. A. L. Spek, *Acta Crystallogr., Section D*, 2009, **65**, 148-155.
35. C. A. Hollis, S. R. Batten and C. J. Sumby, *Cryst. Growth Des.*, 2013, **13**, 2350-2361.
36. M. Wriedt, J. P. Sculley, A. A. Yakovenko, Y. Ma, G. J. Halder, P. B. Balbuena and H.-C. Zhou, *Angew. Chem., Int. Ed.*, 2012, **51**, 9804-9808.
37. P. Nugent, Y. Belmabkhout, S. D. Burd, A. J. Cairns, R. Luebke, K. Forrest, T. Pham, S. Ma, B. Space, L. Wojtas, M. Eddaoudi and M. J. Zaworotko, *Nature*, 2013, **495**, 80-84.